Supporting Information

Effect of Noncovalent Interactions on Ag(I)/Cu(II) Supramolecular Architecture for Dual-functional Luminescent and Semiconductivity Properties

Yang Song[a], Ruiqing Fan[*a], Xi Du[a], Kai Xing[a], Ping Wang[a], Yuwei Dong[a], and Yulin Yang[*a]

[a] MIIT Key Laboratory of Critical Materials Technology for New Energy Conversion and Storage, School of Chemistry and Chemical Engineering, Harbin Institute of Technology, Harbin 150001, P. R. of China

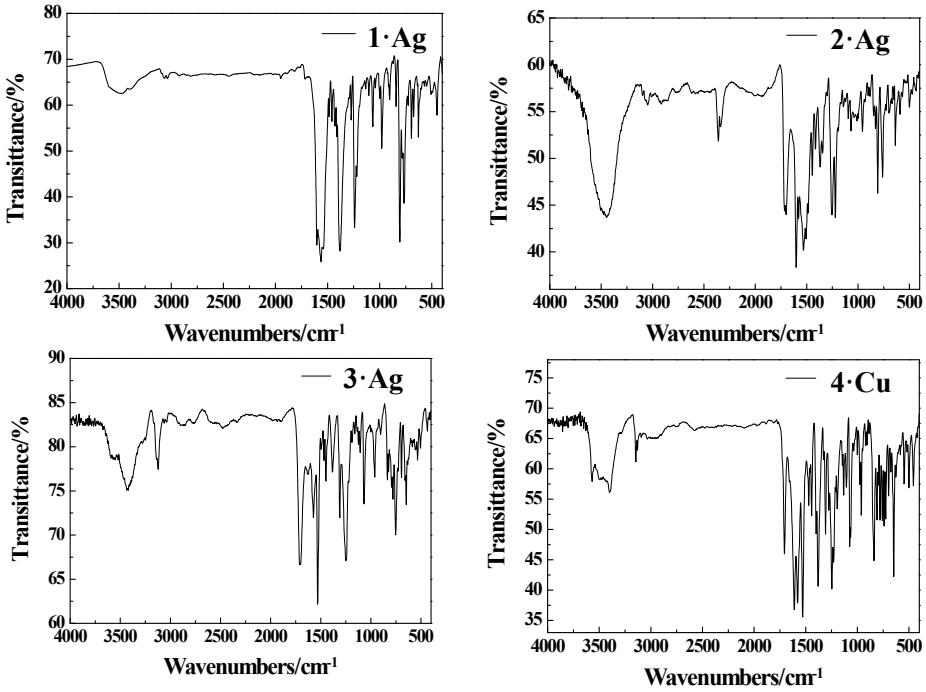

Fig. S1 The IR spectra of **1•Ag, 2•Ag, 3•Ag** and **4•Cu.**

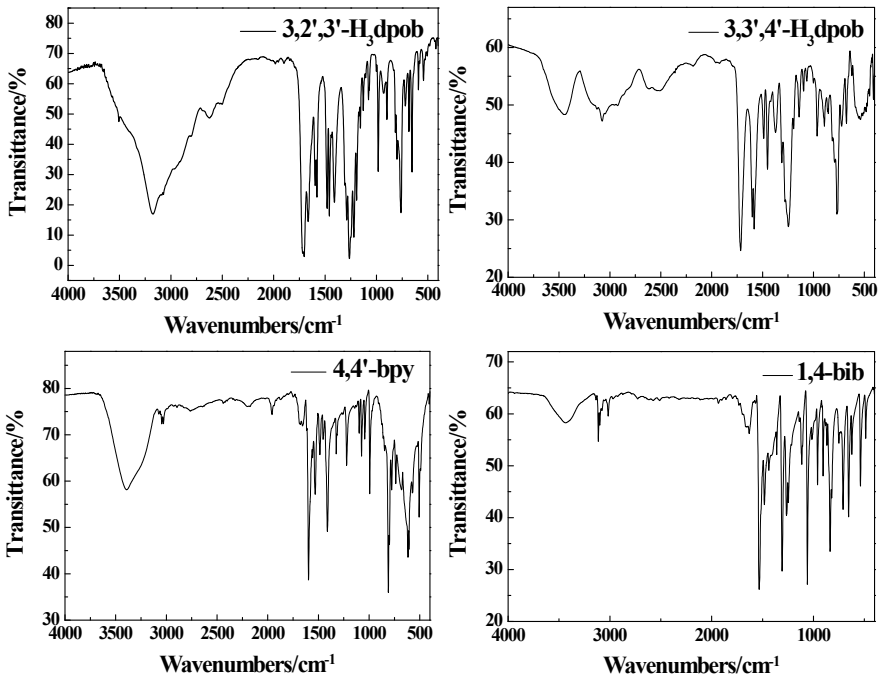

Fig. S2 The IR spectra of 3,2’,3’-H_3dpob, 3,3’,4’-H_3dpob, 4,4’-bpy and 1,4-bib ligands.

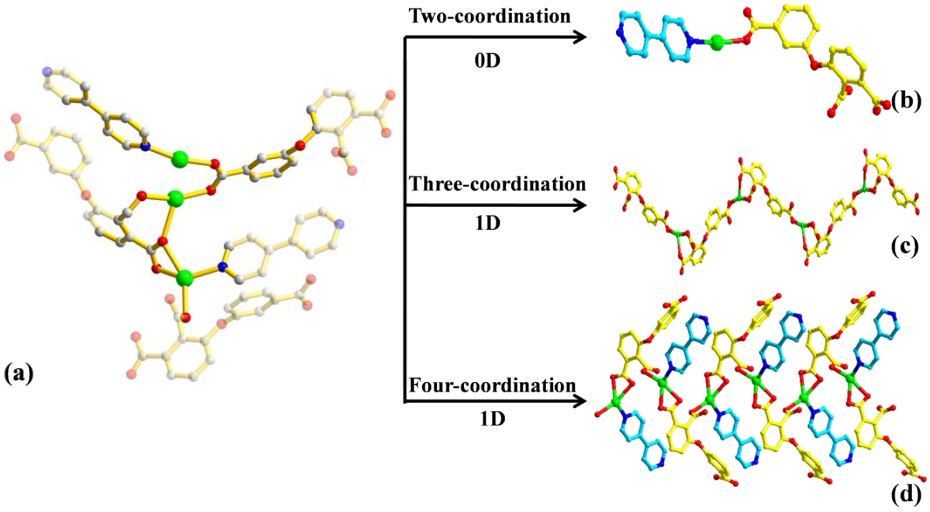

Fig. S3 (a) Asymmetric unit and the asymmetry-operated components in 60% transparency; (b) Two-coordination 0D structure based on Ag1 ion; (c) Three-coordination 1D wave chain based on Ag2 ion; (d) Four-coordination 1D chain based on Ag3 ion.

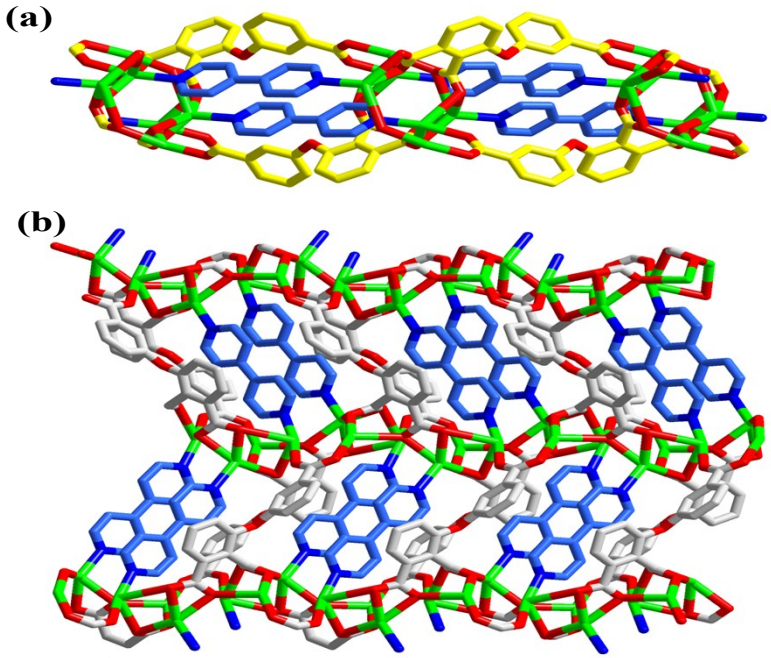

Fig. S4 (a) The illustration of the 2D layer of **1•Ag** along *b* axis; (b) The illustration of the 2D compact layer of **1•Ag** in the *bc* plane.

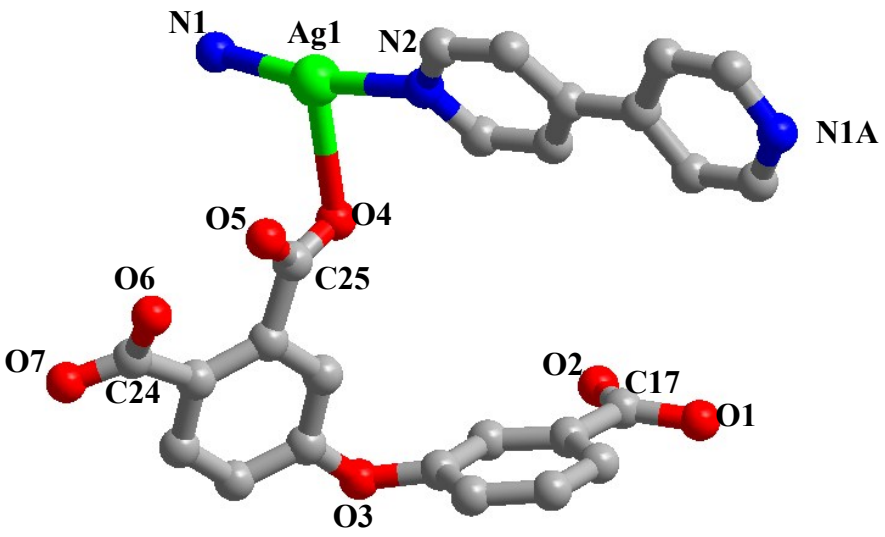

Fig. S5 The structural unit of **2•Ag** with labeling scheme and 50% thermal ellipsoids (hydrogen atoms are omitted for clarity).

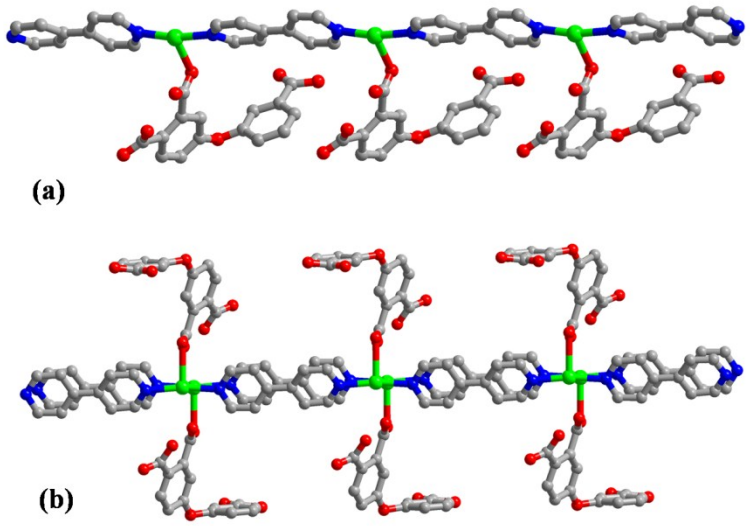

Fig. S6 (a) The 1D chain of **2•Ag**; (b) The 1D double-chain of **2•Ag.**

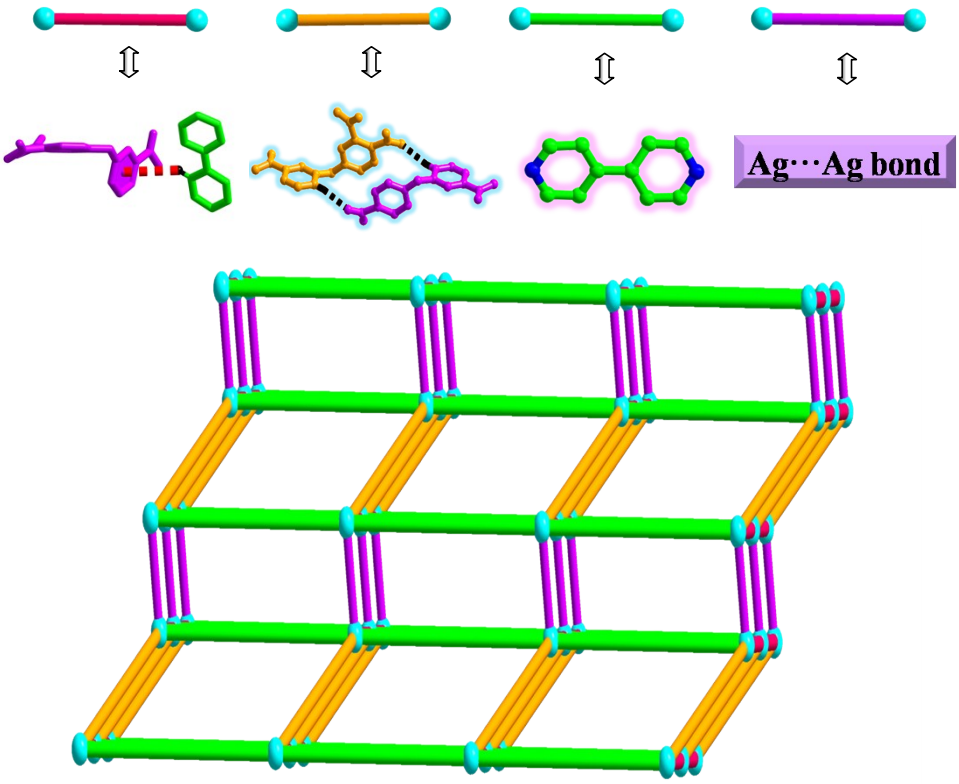

Fig. S7 Topological view of the 3D structure of **2•Ag** with the 6-connected **pcu** net (color code: the silver ions, blue ball; the defined linkers of C−H···O and π···π interactions, rose and yellow sticks; the defined linkers of bpy and Ag···Ag bond, green and purple sticks

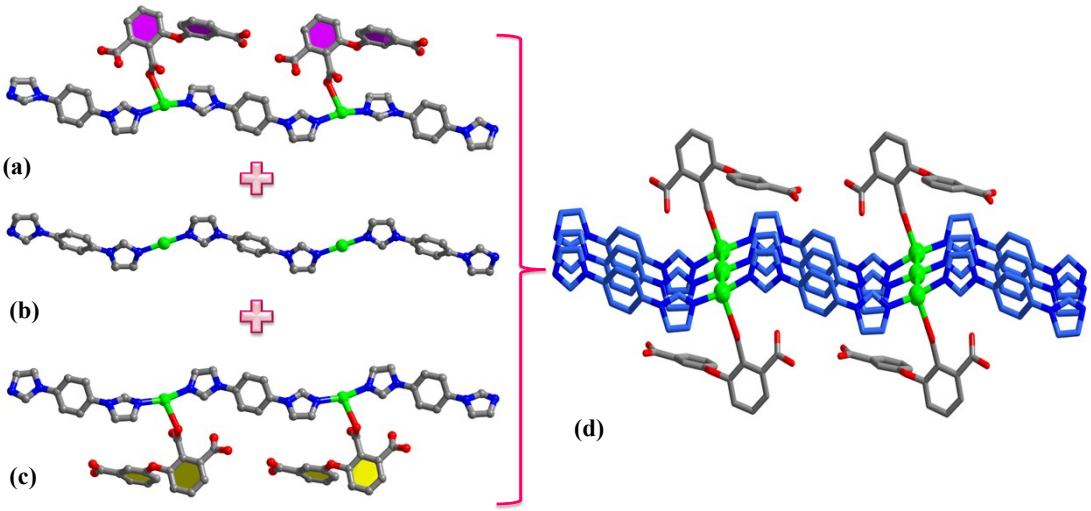

Fig. S8 (a) The three-coordination 1D chain in **3•Ag**; (b) The two-coordination 1D chain in **3•Ag**; (c) The other three-coordination 1D chain in **3•Ag**; (d) The 1D triple chain structure of **3•Ag**.

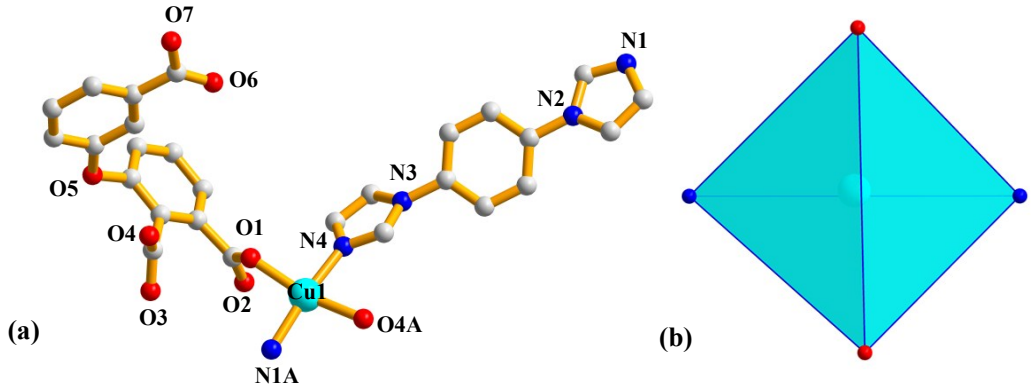

Fig. S9 (a) The structural unit of **4•Cu** with labeling scheme and 50% thermal ellipsoids (hydrogen atoms are omitted for clarity). (b) Polyhedral representation of the coordination sphere of the Cu^{2+} centre.

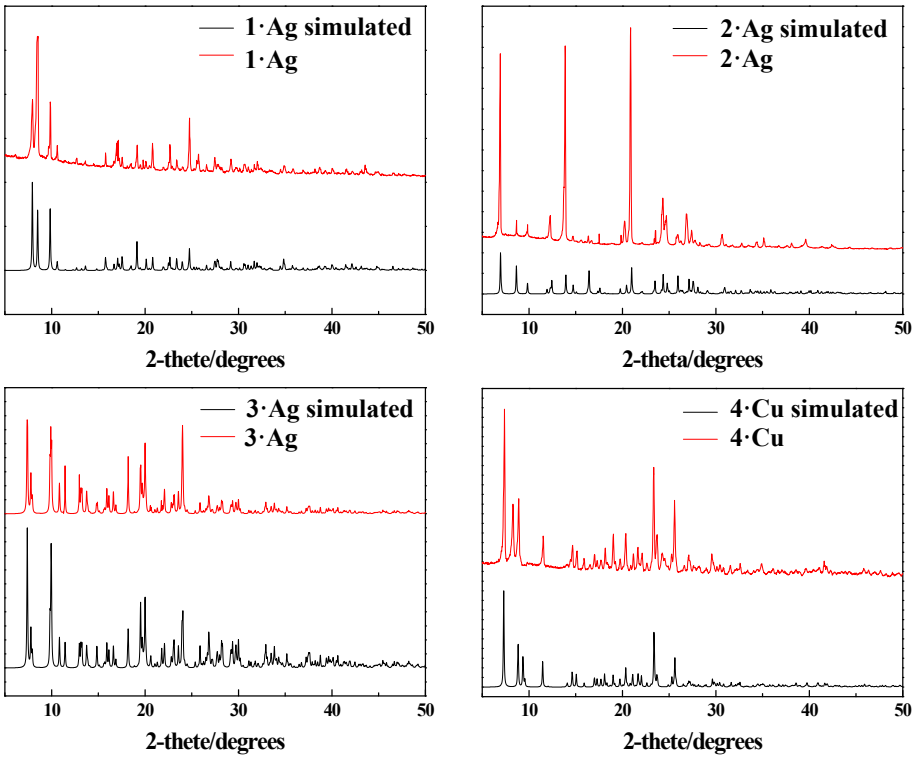

Fig. S10 The PXRD patterns of **1•Ag**, **2•Ag**, **3•Ag** and **4•Cu** with the relevant simulated patterns.

In order to check the phase purity of **1•Ag**, **2•Ag**, **3•Ag** and **4•Cu** the X-ray powder diffraction (PXRD) pattern was checked at room temperature. The simulated and experimental PXRD patterns of **1•Ag**, **2•Ag**, **3•Ag** and **4•Cu** are in good agreement with each other (Fig. S7), indicating the phase purity of the products. The differences in intensity may be due to the preferred orientation of the powder samples.

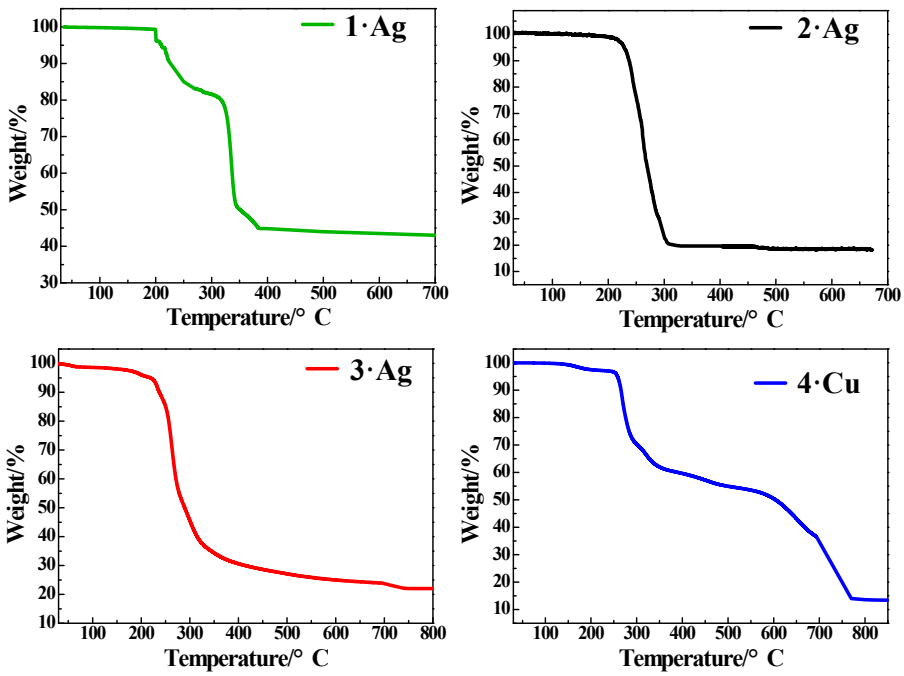

Fig. S11 The TGA curves of compounds **1•Ag, 2•Ag, 3•Ag** and **4•Cu.**

To estimate the stability of the compounds, thermogravimetric analyses (TGA) in purified air were carried out and the TGA curves are shown in Fig. S8. In the TGA curve of **1•Ag**, there are two weight-loss steps. The loss 19.53% occurring at the first step is attributed to the decomposition of bpy 200.1~313.7 °C (calculated 20.02%). The second weight-loss of 37.83% from 313.8 to 393.1 °C, which corresponds to the decomposition of dpob^{3-} (calculated 38.39%). Host framework of **2•Ag** could keep until 216.2 °C and the rapid weight loss occurs from 217.5 to 308.2 °C owing to the decomposition of organic ligands (found 81.08 %, calcd 81.89 %). After further heating, the TGA curve keeps horizontal. For **3•Ag**, the TGA curve displays one continuous weight loss step from 211.8 °C (found 77.99 %, calcd 79.64 %), which is attributed to the decomposition of the framework including the three bib ligands, two H_3dpob ligands and two uncoordinated water molecules. The remaining weight of 42.64% for **1•Ag**, 19.92% for **2•Ag** and 22.01% for **3•Ag**, which is in good agreement with the calculated value (41.59% for **1•Ag**, 19.11% for **2•Ag** and 20.35% for **3•Ag**), indicating that the final product is Ag_2O. In the TGA curve of **4• Cu**, the first weight loss from 252.2 to 339.6 °C is consistent with the decomposition of bib ligand (found 36.62 %, calcd 34.48 %). After further heating, the following smooth weight-loss is

7.45% during 338.2~578.8°C, which is consistent with the removal of uncoordinated 3′-position carboxyl (calculated 7.39%). The last weight loss from 580.5 to 768.7 °C, which is attributed to the decomposion 13.47%, correspond to the percentage (calcd: 13.13%) of Cu and O components, indicating that the final product is CuO.

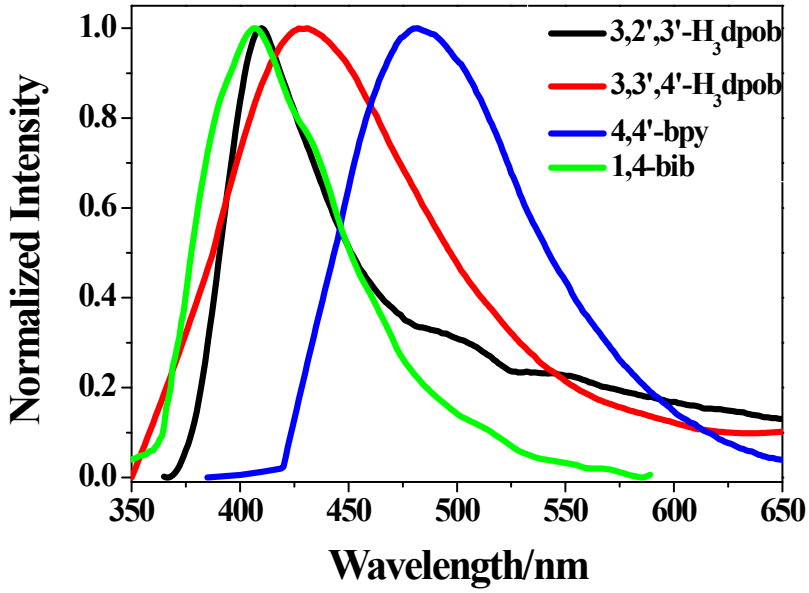

Fig. S12 Emission spectra of ligands 3,2',3'-H_3dpob, 3,3',4'-H_3dpob, 4,4'-bpy and 1,4-bib in the solid state at 298 K.

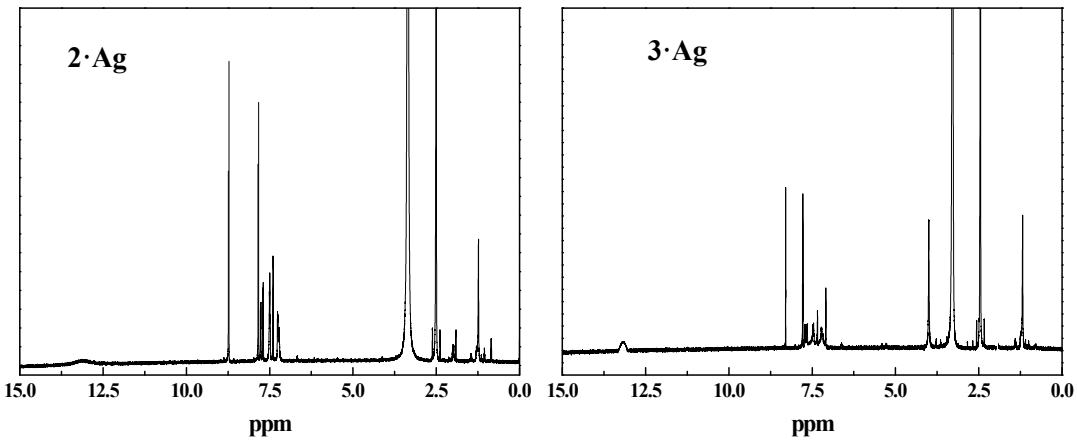

Fig.S13 The ^{1}HNMR spectra of **2•Ag** and **3•Ag**.

Compound **2•Ag**: ^{1}H NMR (400 MHz, DMSO-d_6, Fig. S13†): δ = 13.06 (s, 2H, COO*H*) 8.79 (d, 4 H, Py–$H_{1,5,8,9}$), 7.88 (d, 4 H, Py–$H_{2,4,7,10}$), 7.84 (d, 1 H, Ph–H_{20}), 7.76 (d, 1 H, Ph–H_{23}), 7.69 (d, 1 H, Ph–H_{14}), 7.53 (s, 1 H, Ph–H_{12}), 7.49 (t, 1 H, Ph–H_{15}), 7.39 (d, 1 H, Ph–H_{19}), 7.26 (d, 1 H, Ph–H_{16}) ppm.

Compound **3•Ag**: ^{1}H NMR (400 MHz, DMSO-d_6, Fig. S13†): δ = 13.21 (s, 3 H, –COO*H*), 8.29 (s, 6 H, Imi–$H_{3,7,15,22,25,36}$), 7.79 (s, 6 H, Imi–$H_{2,8,14,23,26,34}$), 7.78 (d, 12 H, Ph–$H_{5,6,11,12,17,18,20,21,29,30,32,33}$), 7.72 (d, 2 H, Ph–$H_{38,53}$), 7.65 (d, 2 H, Ph–$H_{48,63}$), 7.45 (t, 4 H, Ph–$H_{39,50,54,65}$), 7.33 (s, 2 H, Ph–$H_{40,55}$), 7.23 (d, 2 H, Ph–$H_{47,62}$), 7.18 (s, 2 H, Ph–$H_{46,61}$), 7.08 (s, 6 H, Imi–$H_{1,9,13,24,27,35}$) ppm.

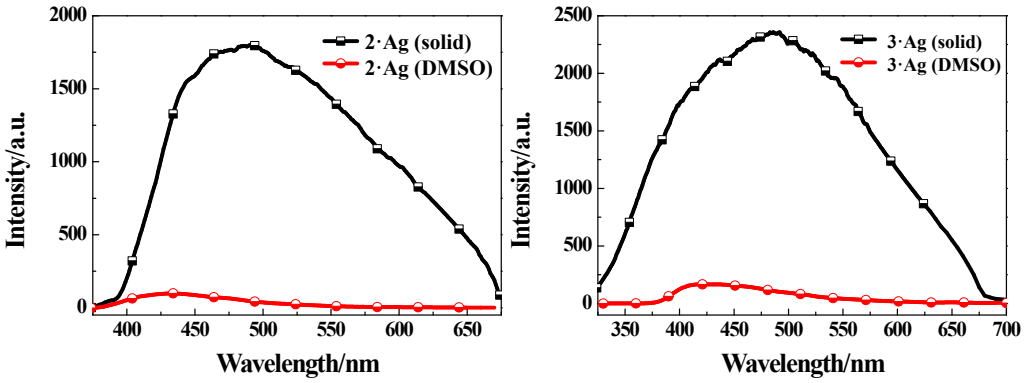

Fig. S14 The comparative solid state and solution (DMSO) luminescence intensities for compounds **2•Ag** and **3•Ag**.

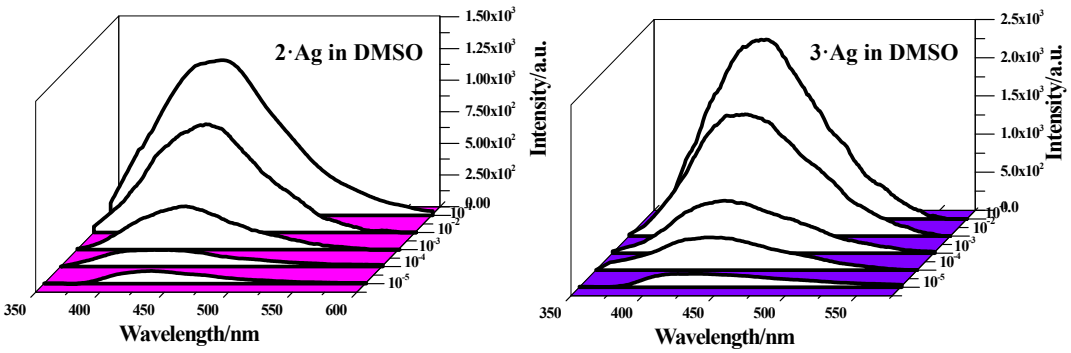

Fig. S15 Luminescence intensities of compounds **2•Ag** and **3•Ag** in DMSO at different concentrations.

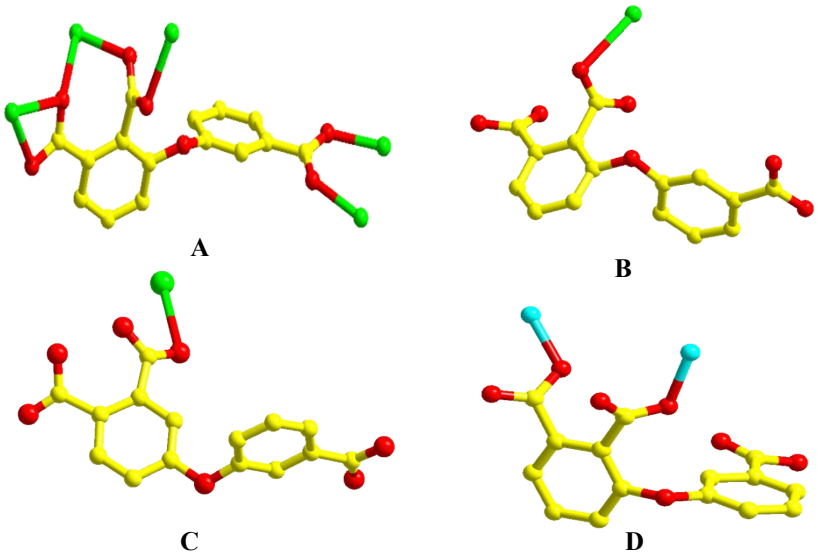

Scheme S1 Coordination modes and configurations of H_3dpob ligands in compounds **1•Ag, 2•Ag, 3•Ag** and **4•Cu**.

Firstly, when using the same reaction mixtures ($AgNO_3$ and bpy), the coordination mode of 3,2',3'-H_3dpob is different from 3,3',4'-H_3dpob completely, owing to the effects of carboxylate positions (Scheme 2 A and B). For **1•Ag**, 3,2',3'-H_3dpob ligand shows a *cis*-typed configuration with μ_5-bridging mode, and 3-, 2'-, and 3'-carboxylic groups exhibit μ_2-η^1-η^1, μ_2-η^1-η^1, and μ_2-η^2-η^1 coordination mode, respectively. Due to the rich way of coordination, unique 2D compact structure has been obtained. However, in **2•Ag**, 3,3',4'-H_3dpob in a *trans*-typed configuration possesses μ_1-bridging mode with 3'-carboxylic group in a monodentate coordination mode, which results in forming a 1D chain structure. Secondly, compounds **1•Ag** and **3•Ag** imply the influence of the secondary ligands on the resulting frameworks. The length of the rigid auxiliary ligand is increased from 7.06 Å (bpy) to 9.86 Å (bib), and changing the modes of the 3,2',3'-H_3dpob ligand from μ_5 to μ_1 (Scheme 2A and C), *cis*- and *trans*-type configurations have been observed for each connection, which finally generate different 2D and 1D structure. Thirdly, the same reaction mixtures (3,2',3'-H_3dpob and bib) were subjected to different synthetic routes by varying metal ions to form diverse architectures in **3•Ag** and **4•Cu**. Comparison of Cu(II) to Ag(I), their ionic radium and valance state are distinct different, which may lead to diversity in bond strength, bond lengths and bond angles even with the same organic ligands forming the covalent bonds.

Table S1 Selected bond lengths [Å] and angles [°] for **1•Ag**, **2•Ag, 3•Ag** and **4•Cu**.

Bond length	(Å)	Bond angle	(°)	Bond angle	(°)
1•Ag					
Ag(1)-O(6)	2.152(3)	O(6)-Ag(1)-O(1)	157.27(10)	Ag(1)-Ag(2)-Ag(3)	150.004(16)
Ag(1)-O(1)	2.193(3)	O(6)-Ag(1)-O(4)#1	120.74(10)	N(2)-Ag(3)-O(2)	104.55(10)
Ag(1)-O(4)#1	2.538(4)	O(1)-Ag(1)-O(4)#1	76.91(10)	N(2)-Ag(3)-O(4)	104.25(11)
Ag(1)-Ag(2)	2.9665(6)	O(6)-Ag(1)-Ag(2)	84.71(8)	O(2)-Ag(3)-O(4)	148.55(11)
Ag(2)-O(5)	2.163(3)	O(1)-Ag(1)-Ag(2)	72.57(7)	N(2)-Ag(3)-O(3)	123.43(10)
Ag(2)-N(1)	2.166(3)	O(4)#1-Ag(1)-Ag(2)	132.49(8)	O(2)-Ag(3)-O(3)	118.15(9)
Ag(2)-Ag(3)	3.0649(6)	O(5)-Ag(2)-N(1)	164.57(12)	O(4)-Ag(3)-O(3)	52.11(9)
Ag(3)-N(2)	2.257(3)	O(5)-Ag(2)-Ag(1)	74.96(8)	N(2)-Ag(3)-Ag(2)	137.48(8)
Ag(3)-O(2)	2.351(3)	N(1)-Ag(2)-Ag(1)	110.04(8)	O(2)-Ag(3)-Ag(2)	59.46(7)
Ag(3)-O(4)	2.469(3)	O(5)-Ag(2)-Ag(3)	75.07(8)	O(4)-Ag(3)-Ag(2)	105.07(7)
Ag(3)-O(3)	2.500(3)	N(1)-Ag(2)-Ag(3)	98.64(8)	O(3)-Ag(3)-Ag(2)	58.85(6)
2•Ag					
Ag(1)-N(2)#1	2.167(4)	N(2)#1-Ag(1)-N(1)	168.88(16)	N(1)-Ag(1)-Ag(1)#2	86.75(12)
Ag(1)-N(1)	2.183(4)	N(2)#1-Ag(1)-O(4)	94.59(16)	O(4)-Ag(1)-Ag(1)#2	102.44(11)
Ag(1)-O(4)	2.689(4)	N(1)-Ag(1)-O(4)	91.39(16)	N(2)#1-Ag(1)-Ag(1)#2	101.07(12)
Ag(1)-Ag(1)#2	3.451(9)				
3•Ag					
Ag(1)-N(3)	2.076(12)	N(3)-Ag(1)-N(1)	179.7(7)	O(5)-Ag(2)-Ag(1)	103.4(3)
Ag(1)-N(1)	2.081(14)	N(3)-Ag(1)-Ag(2)	100.4(4)	N(9)-Ag(2)-Ag(1)	85.6(4)
Ag(1)-Ag(2)	3.150(3)	N(1)-Ag(1)-Ag(2)	79.8(4)	N(5)-Ag(2)-Ag(1)	108.6(3)
Ag(1)-Ag(3)#1	3.153(3)	N(3)-Ag(1)-Ag(3)#1	79.6(4)	N(8)#2-Ag(3)-N(12)	160.7(6)
Ag(2)-N(9)	2.174(13)	N(1)-Ag(1)-Ag(3)#1	100.2(4)	N(8)#2-Ag(3)-O(12)	90.9(4)
Ag(2)-N(5)	2.177(13)	Ag(2)-Ag(1)-Ag(3)#1	179.93(9)	N(12)-Ag(3)-O(12)	97.9(5)
Ag(2)-O(5)	2.638(10)	N(9)-Ag(2)-N(5)	159.9(5)	N(8)#2-Ag(3)-Ag(1)#1	84.8(3)
Ag(3)-N(8)#2	2.163(14)	N(9)-Ag(2)-O(5)	91.3(4)	N(12)-Ag(3)-Ag(1)#1	109.5(4)
Ag(3)-N(12)	2.175(14)	N(5)-Ag(2)-O(5)	98.9(5)	O(12)-Ag(3)-Ag(1)#1	103.3(3)
Ag(3)-O(12)	2.652(10)				
Ag(3)-Ag(1)#1	3.153(3)				
4•Cu					
Cu(1)-O(1)	1.951(3)	O(1)-Cu(1)-O(4)#1	161.87(12)	O(1)-Cu(1)-N(4)	91.12(13)
Cu(1)-O(4)#1	1.965(3)	O(1)-Cu(1)-N(1)	93.58(13)	O(4)#1-Cu(1)-N(4)	85.37(13)
Cu(1)-N(1)	1.972(3)	O(4)#1-Cu(1)-N(1)	92.49(13)	N(1)-Cu(1)-N(4)	170.87(15)
Cu(1)-N(4)	1.986(3)				

Symmetry transformations used to generate equivalent atoms: #1: –x, –y+2, –z; #2: –x, –y+1, –z+1.

Table S2 The Dihedral Angles for **1•Ag, 2•Ag, 3•Ag** and **4•Cu.**

Compounds	Dihedral angle between of the plane three atomic carboxylic group and its benzene ring (°)			Dihedral angle between the two benzene rings (°)
1•Ag	3-carboxylic group	2'-carboxylic group	3'-carboxylic group	
	16.32°	85.09°	18.59°	76.73°
2•Ag	3-carboxylic group	3'-carboxylic group	4'-carboxylic group	
	10.28°	30.19°	24.08°	75.62°
3•Ag	3-carboxylic group	2'-carboxylic group	3'-carboxylic group	
	3.18°	69.60°	34.32°	79.41°
4• Cu	3-carboxylic group	2'-carboxylic group	3'-carboxylic group	
	7.39°	54.09°	52.73°	88.12°

Table S3 Summary of the luminescent properties of Ag(I) compounds.

No.	Cite	Complex	Excitation and emission (compounds)	Excitation and emission (ligands)	Assignment
1	*CrystEng Comm,* 2015, 17, 5538	$\{[Ag(HDSPTP)]\cdot 30H_2O\}_n$ (3) $\{[Ag(HDSPTP)(H_2O)]\cdot 3H_2O\}_n$ (4), $[Ag_2(DSPTP)]_n$ (5), $\{[Ag_4(DSPTP)_2(H_2O)_3]\cdot 2H_2O\}_n$ (6) (H_2DSPTP=4'-(2,4-disulfophenyl)-4,2':6',4''-terpyridine	λ_{ex} = 357 nm for 3 λ_{em} = 430 nm λ_{ex} = 366 nm for 4 λ_{em} = 488 nm λ_{ex} = 336 nm for 5 λ_{em} = 446 nm λ_{ex} = 333 nm for 6 λ_{em} = 460 nm	HDSPTP λ_{em} = 430 nm	The ligand-centered nature of the emission because the d^{10} ions are difficult to oxidize or reduce.
2	*Cryst. Growth Des*. 2014, 14, 2230	$[Ag_2(bpz)_4(mal)\cdot 7H_2O]_n$ (1L and 1R) , $[Ag_4(bpz)_5(glu)_2]_n$ (3), $[Ag_4(bpz)_5(adip)_2]_n$ (4), $[Ag_4(bpz)_7(pim)_2\cdot 12H_2O]_n$ (5),$[Ag_2(bpz)_4(sub)\cdot 7H_2O]_n$(6), $[Ag_2(bpz)_3(aze)\cdot 3.5H_2O]_n$ (7) (H_2mal = malonic acid, H_2suc = succinic acid, H_2glu = glutaric acid, H_2adip = adipic acid, H_2pim = pimelic acid, H_2sub = suberic acid, H_2aze = azelaic acid)	298 K λ_{ex} = 365 nm λ_{em} = ca. 465 nm for 1, 3, 4, 6, and 7 λ_{em} = 454 nm for 5 77 K Enhanced but no obvious emission shifts	bpz λ_{em} = 342 nm	Ligand-centered transitions
3	*Chem. Commun.,* 2014, 50, 9000	$[Ag_2(Hpidc)(NH_3)_2]$ (1), $[Ag_2(Hpidc)(NH_{3)2}]_2\cdot 2H_2O$ (2), $[Ag_4(Hpidc)_2(en)_2]$ (3) $[Ag_4(Hpidc)_2(pn)_2]$ (4) NH_3=ammonia en=1,2-diaminoethane pn=1,3-diaminopropane	λ_{ex} = 250 nm High energy emission is 400 nm Low energy emission is 550 nm	H_3pidc λ_{em} = 300 nm	HE bands probably result from intra-ligand n–π or π–π transitions in $Hpidc^{2-}$

					LE emissions should be phosphorescence
4	*Cryst. Growth Des.*, 2014, 14, 4674	$[Ag_2(\mu_4\text{-bztpy})\{Ag(CN)_2\}_2]\cdot EtOH$(1) $[Ag(\mu_3\text{-bztpy})\{Ag(CN)_2\}]$ (2)	λ_{ex} = 471 nm(1) and 479nm(2) λ_{em} = 538 nm(1) and 547nm(2)	bztpy λ_{ex} = 332 nm and 450 nm λ_{em} = 378 nm and 534 nm	Intraligand transition
5	*Cryst. Growth Des.* 2014, 14, 1888	$[Ag_3L_2(H_2O)_2](NO_2)_3\cdot 10H_2O$, $[Ag_3L_2(H_2O)_2](NO_3)_3\cdot 4CH_3OH\cdot 4H_2O$ $[Ag_3(NO_3)_2L_2](NO_3)\cdot C_2H_5OH\cdot 3H_2O$ N,N′,N″-Tris(2-pyridinylethyl)-1,3,5-benzenetricarboxamide (L)	λ_{ex} = 255 nm λ_{em} = 399, 365 and 366 nm	L λ_{ex} = 255 nm λ_{em} = 400 nm	closed-shell argentophilic (d^{10}–d^{10}) interactions
6	*CrystEng Comm,* 2014, 16, 3015	$[Ag(Htzsuc)]_n$ (1, H_2tzsuc = 2-(1H-1,2,4-triazol-1-yl)succinic acid)	λ_{ex} = 330 nm λ_{em} = 467 nm		The charge transfer transition between ligands and metal centers and/or intraligand fluorescence emission
7	*CrystEng Comm*, 2014, 16, 5110	$[Ag_2(hpyb)_{0.5}(L_1)_{0.5}(NO_3)]\cdot H_2O$(1), $[Ag_4(hpyb)(HL_2)(NO_3)_2]\cdot 2H_2O$(2), $[Ag_3(hpyb)_{0.5}(L_3)(NO_3)]$(3), $[Ag_6(hpyb)(L_4)_2(NO_3)]\cdot NO_3\cdot 2H_2O$ (4) $[Ag_5(hpyb)_{0.5}(L_5)_2(NO_3)]\cdot H_2O$(5), $\{Ag_4(hpyb)[L_6(CH_3)_2]_2\}$(6), $\{Ag_6(hpyb)(HL_7)_2[L_7(CH_3)]\}$(7) $[Ag_3(hpyb)_{0.5}(HL_8)]\cdot H_2O$ (8) (H_2L_1=p-phthalic acid, H_3L_2= 1,2,3-benzenetricarboxylic acid, H_2L_3 =cis-2-butenedioic acid, H_2L_4 = 2,3-pyridinedicarboxylic acid,	λ_{ex} = 370 nm λ_{em} = 514, 590, 546, 522, 516, 572, 524 and 588 nm	Hpyb λ_{ex} = 343 nm λ_{em} = 529 nm	Ligand-based luminescence.

		H_2L_5 = m-phthalic acid, H_4L_6 = 1,2,4,5-benzenetetracarboxylic acid, H_3L_7 = 1,2,4-benzenetricarboxylic acid and H_4L_8 = 4,4′-oxydiphthalic acid)			
8	*Dalton Trans.*, 2014, 43, 8774	$[Ag_2(dpb)_2(bdc)\cdot 9H_2O]_n$ (1)	λ_{ex} = 365 nm λ_{em} = 419 nm	dpb λ_{ex} = 300 nm λ_{em} = 367 nm	The intraligand π*→π transition
9	*Inorg. Chim. Acta*, 2014, 415, 61	$[Ag_2(mpyz)(ipa)]_n$ (1) $[Ag_3(mpyz)(btc)]_n$ (2) $[Ag_4(apyz)_2(ipa)\cdot 0.5DMF]_n$ (3) $[Ag_3(apyz)_2(btc)]_n$ (4) methylpyrazine (mpyz), aminopyrazine (apyz), isophthalic acid (H_2ipa), 1,3,5-benzenetricarboxylic acid (H_3btc)	λ_{ex} =300 nm. λ_{em} = 415 and 517 nm for 1 λ_{em} = 512 nm for 2 λ_{em} = 411 nm for 3 λ_{em} = 411 and 498 nm for 4	apyz λ_{em} = 422 nm H_2ipa λ_{em} = 350 nm H_3btc λ_{em} = 358 and 496 nm	Intraligand π/*π transition. intraligand fluorescent emission π/*n or π/*π transitions.
10	*RSC Adv.*, 2012, 2, 8421	$\{[Ag(L_1)(CH_3CN)][Ag(L_1)(OTf)](OTf)\}_n$ (1) $\{[Ag(L_2)](OTf)(H_2O)\}_n$ (2) bis(pyridine-3-ylmethyl)terephthalate (L_1)	λ_{ex} = 284 nm for 1 λ_{em} = 398 nm for 1 Another excitation wavelength λ_{ex} = 350 nm for 1 λ_{em} = 482 nm for 1 λ_{ex} = 284 nm for 2 λ_{em} = 361 nm for 2	λ_{ex} =284 nm for L_1 λ_{em} =326 nm for L_1 λ_{ex} = 284 nm for L_2 λ_{em} =326 nm for L_2	Argentophilic cluster centred emission π*–π and/or π*–π transmissions
11	*CrystEng Comm*, 2012, 14, 480	$\{[Ag(bga)(pzc)]\cdot 0.5H_2O\}_n$(1) $[Ag_2(bga)_2(pzdc)(H_2O)]_n$(2) bga=benzoguanamine, Hpzc =pyrazine-2-carboxylic acid, H_2pzdc = pyrazine-2,3-dicarboxylic acid	λ_{ex} = 280 nm λ_{em} = 400 to 470 nm for 1 λ_{em} = 422 nm for 2	bga λ_{ex} = 280 nm λ_{em} = 376 and 435 nm	Ag(I)-perturbed intraligand (IL) π→π* transition
12	*Inorg. Chem. Commun.*, 2012, 24, 73	$[Ag(Hcpob)(bpy)]_n$ (1) 4-(3′-carboxylphenoxy)benzoic acid (H_2cpob), 4,4′-bipyridine (bpy)	λ_{ex} = 330 nm λ_{em} = 412 nm and 465 nm	H_3dpob λ_{ex} = 330 nm λ_{em} = 465 nm	π→π* intraligand transitions or the LMCT
13	*CrystEng*	$\{Ag_8(MDIP)_2(m\text{-}bix)\}_n$(2) (m-	λ_{ex} = 356 and 397 nm	H_4MDIP	Intraligand π–

	Comm, 2011, 13, 1314	bix=1,3-bis(imidazol-1-ylmethyl)-benzene)	λ_{em} = 469 nm	λ_{ex} = 350 nm λ_{em} =495 nm	π* transitions
14	*CrystEng Comm*, 2008,10,1866	$[Ag_2(L_2)(NO_3)_2]_n$ (2) 1,3-bis(triazol-1-ylmethyl)benzene (L_2)	λ_{ex} = 278 nm λ_{em} = 383 nm	L_2 λ_{ex} = 276 nm λ_{em} = 378 nm	Intra-ligand (n–π* or π–π*) emission
15	*Inorg.Chem.*, 2005, 44, 1031	$[Ag_2(bmsb)(ClO_4)_2]$ (1), $[Ag_2(bmsb)(H_2O)_4](BF_4)_2$(2), $[Ag_2(bdb)(CF_3SO_3)_2]$ (3) (bmsb=1,4-bis(methylstyryl)benzene, bdb=4,4'-bis(2,5-dimethylstryryl)biphenyl)	λ_{ex} = 446 nm for 1 λ_{em} = 485 nm for 1 λ_{ex} = 444 nm for 2 λ_{em} = 488 nm for 2 λ_{ex} = 448 nm for 3 λ_{em} = 477 nm for 3	bmsb λ_{ex} = 418 nm λ_{em} =453,472nm bdb λ_{ex} = 419 nm λ_{em} =422,462 nm	π-π*